THE JOURNAL OF PHYSICAL CHEMISTRY C

Article

pubs.acs.org/JPCC

Surface Electric Fields of Aqueous Solutions of NH_4NO_3, $Mg(NO_3)_2$, $NaNO_3$, and $LiNO_3$: Implications for Atmospheric Aerosol Chemistry

Wei Hua, Dominique Verreault, and Heather C. Allen*

Department of Chemistry & Biochemistry, The Ohio State University, 100 West 18th Avenue, Columbus, Ohio 43210, United States

Supporting Information

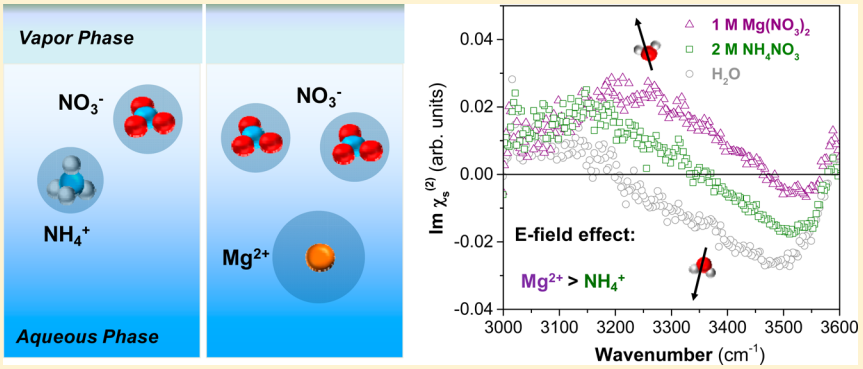

ABSTRACT: Ammonium (NH_4^+), magnesium (Mg^{2+}), sodium (Na^+), and nitrate (NO_3^-) ions are common constituents of ocean waters and found in abundance in marine atmospheric aerosols. Revealing the surface propensity (surface activity) of relevant ions provides insight into heterogeneous aerosol processes and potential impact on atmospheric chemistry. However, there is sparse surface data on NH_4^+, Mg^{2+}, and little consensus for nitrate's surface activity. Phase-resolved vibrational sum frequency generation (VSFG) experiments are highly well-suited for this task; yet, only aqueous $NaNO_3$ salt has been studied by this technique to date. Here we investigate NH_4^+, Mg^{2+}, and Na^+, in addition to lithium (Li^+), to fully understand the effect of countercations on nitrate but also to elucidate the surface propensity of the countercations themselves as this is the first phase-resolved heterodyne-detected (HD-)VSFG study to address nitrate with countercations beyond sodium. We show the presence of an interfacial electric field generated by surface-active NO_3^- and its counterions, including NH_4^+, a cation that is commonly identified with nitrate in tropospheric aerosol generated in urban regions. We find that NH_4^+, Li^+, Na^+, and Mg^{2+} are less surface-active relative to NO_3^-, with Mg^{2+} being the least so. The cation identity and the ion concentration determine the magnitude of this electric field, which decreases in the order of $Mg^{2+} > Na^+ > Li^+ > NH_4^+$ at the ~2 M NO_3^- concentration (highly relevant to low water content aerosol). Important to note is that the surface charge density does not completely dictate the trend observed as one might expect.

INTRODUCTION

Ions residing at the air/water interface can drive heterogeneous chemistry of atmospheric aerosols.[1−7] Yet, surface propensity, or surface activity, of ions is not well understood, although this phenomenon has a major impact on aerosol and ocean surface processing,[8,9] ice/snowpack chemistry,[10−13] and thundercloud electrification,[14] in addition to other environmental processes such as capillary geochemical processes in unsaturated zones of soils.[15−17] Here we focus on understanding the surface propensity and the interfacial ion distributions of ammonium (NH_4^+), magnesium (Mg^{2+}), sodium (Na^+), and lithium (Li^+) with that of the counteranion nitrate (NO_3^-). Although there has been some work on NO_3^- with Na^+ using phase-sensitive vibrational sum frequency generation (PS-VSFG),[18] there have been no phase-resolved VSFG studies on the other ions in combination with NO_3^- even though NH_4^+ and Mg^{2+} are key atmospheric species. It is well-known that NH_4^+, Mg^{2+}, and Na^+ are pervasive cations in atmospheric aerosols,[19,20] while Na^+ and Mg^{2+} are the most common cations in seawater.[21] Yet, relatively few studies have included explicit discussion of counter-cations[22−30] or the cation itself.[25]

In addition to the abundance of specific cations in atmospheric aerosols such as NH_4^+, Mg^{2+}, and Na^+, NO_3^- ions, along with chloride (Cl^-), bromide (Br^-), sulfate (SO_4^{2-}), and bisulfate (HSO_4^-) ions, are also abundant in aerosols and terrestrial water sources.[3,21,31] Gaseous ammonia (NH_3) reacts with nitric acid (HNO_3) in the atmosphere, a product of the heterogeneous hydrolysis of NO_2, and forms NH_4NO_3, an important semi-volatile component in aerosols.[32−34] Nitrate-containing aerosols can also be formed via reactions of mineral dust aerosols with gas phase nitrogen oxides (NO_x).[35] NO_3^- ions additionally play a crucial role in ice and snowpack chemistry by acting as a source of

Received: June 10, 2014
Revised: October 3, 2014
Published: October 6, 2014

NO_x and OH radicals via photolysis.[36−39] The resulting fluxes of NO_x and OH radicals from ice and snow impact the chemistry of the atmospheric boundary layer. In marine regions, NO_3^- ions are generated by heterogeneous reactions of sea salt aerosols. NaCl and $MgCl_2$ react with HNO_3, NO_3 radicals, N_2O_5, and $ClONO_2$,[31,35,40] resulting in the generation of $NaNO_3$ and $Mg(NO_3)_2$ in/on aerosols and the significant Cl^- ion depletion in sea salt aerosols, as well as yielding photochemically active gaseous halogen products. These reactions are strongly associated with tropospheric ozone formation through reactions with volatile organic compounds (VOCs).[3,31]

In order to gain molecular insight into the interfacial partitioning of NO_3^- ions at the air/aqueous interface, a number of theoretical studies have been published over the past decade. Salvador et al. predicted that NO_3^- anions prefer interfacial over bulk solvation,[41] while Dang et al. found that the probability of finding NO_3^- anions at the aqueous interface is low.[42] This apparent contradiction has since been attributed to the different treatment of NO_3^- polarizability. Additionally, these simulations were done without including countercations. More recently, MD simulations have taken into account the effect of countercations on the interfacial NO_3^- ion distribution. Thomas et al. predicted that NO_3^- anions reside primarily in the bulk, and only a small concentration exists at the air/aqueous interface of $NaNO_3$ solution.[43] Similarly, Minofar et al. also reported for $Mg(NO_3)_2$ solution a very weak surface propensity for NO_3^- ions.[44] Considering the critical role that NO_3^- ions play in various aspects of atmospheric chemistry, it still remains unclear how the countercation identity affects the surface propensity of NO_3^-, or the relative surface propensity of the countercations themselves, in particular for relevant ions such as NH_4^+ and Mg^{2+}.

Concurrently, several experimental studies using electrospray ionization-mass spectrometry (ESI-MS),[45] depth-resolved X-ray photoemission spectroscopy (DR-XPS),[46] IR photodissociation spectroscopy,[47] and glancing-angle Raman spectroscopy[48] have provided information about the surface propensity of NO_3^- ions at air/aqueous interfaces. In addition, other experiments utilizing surface-sensitive nonlinear optical techniques such as SHG[49] and VSFG spectroscopy[50−53] have investigated the presence of interfacial NO_3^- ions and/or their impact on the water hydrogen-bonded network. Otten et al. confirmed the existence of NO_3^- ions in the interfacial region of $NaNO_3$ salt solutions but no strong enhancement in their concentration.[49] Using VSFG spectroscopy, Schnitzer et al. looked at the effect of interfacial NO_3^- ions (of $NaNO_3$) on the water OH stretching region (3000−3800 cm^{-1}).[54] It was found that at low concentrations (~0.6 M) the hydrogen-bonded region (3000−3600 cm^{-1}) remains unaffected by NO_3^- ions, but the dangling OH peak (~3700 cm^{-1}) of the topmost water molecules is slightly perturbed relative to neat water (~25% intensity decrease). This was interpreted as an indication of the presence of near-surface contact ion pairs (with the NO_3^- anions closer to the surface) tying up the dangling OH groups. More recently, using PS-VSFG spectroscopy, Tian et al. obtained a ranking of ion surface propensity of a series of selected aqueous salt solutions; again, Na^+ was selected as the countercation to NO_3^-.[18] There have been no other VSFG studies on nitrate salts other than $NaNO_3$ except that from Allen and co-workers of aqueous $Mg(NO_3)_2$, $Ca(NO_3)_2$, and $Sr(NO_3)_2$.[27] These nitrate-mode and hydrogen-bonding studies suggested that NO_3^- ions, and their corresponding ion pairs, approach the aqueous surface and that interfacial ion pairing between NO_3^- and divalent cations (Mg^{2+}, Ca^{2+}, Sr^{2+}) followed the trend of increasing inversely with the cation charge density.[55]

In the work presented here, selected nitrate salt solutions ($LiNO_3$, $NaNO_3$, NH_4NO_3, and $Mg(NO_3)_2$) and their interfacial ion distributions are investigated using VSFG and HD-VSFG spectroscopy. From our VSFG results, interfacial water organization is perturbed for $LiNO_3$, $NaNO_3$, and $Mg(NO_3)_2$ solutions, whereas NH_4NO_3 showed a smaller effect across the OH stretching region. $Mg(NO_3)_2$ showed the strongest effects including changes to the dangling OH mode associated with topmost located water molecules with respect to salt concentration. Moreover, regardless of the nitrate salt solution, the HD-VSFG Im $\chi_s^{(2)}(\omega_{IR})$ spectra reveal the presence of a positive interfacial electric field in which the direction is governed by the ionic double layer formed by the cation and the NO_3^-, where the cations are consistently observed below the nitrate ion distribution. The cation specificity dictates the magnitude of this electric field, with Mg^{2+} clearly having the strongest effect. Moreover, the divalency of Mg^{2+} has a distinct impact on the nitrate and the surface electric field. Note that no VSFG ($|\chi_s^{(2)}|^2$) results have been reported for NH_4NO_3 and $LiNO_3$, and for phase-resolved VSFG, no results have been reported for NH_4NO_3, $LiNO_3$, or $Mg(NO_3)_2$.

EXPERIMENTAL SECTION

Materials. $LiNO_3$ (>99%, Fisher Scientific, ACS certified powder), $NaNO_3$ (Fisher Scientific, ≥99% colorless crystals, Fisher BioReagents), NH_4NO_3 (MP Biomedicals, ultrapure grade, >99%), and $Mg(NO_3)_2{\cdot}6H_2O$ (Fisher Scientific, ACS grade, >98%) were used in this study. Ultrapure water with a resistivity of 18.2−18.3 MΩ·cm, and a measured pH of 5.6 (the pH value is slightly acidic due to the dissolution of gaseous CO_2) was obtained from a Barnstead Nanopure system (model D4741, Thermolyne Corporation) with additional organic removing cartridges (D5026 Type I ORGANICfree Cartridge Kit; Pretreat Feed).

Salt Solution Preparation. Stock solutions for VSFG measurements were prepared by dissolving salts in ultrapure water and then by filtering them four to six times using activated carbon filters (Whatman Carbon Cap 75, Fisher Scientific) to completely eliminate organic impurities.[56] Raman calibration curves were generated for each nitrate salt solution in order to determine the concentration following filtration (Supporting Information). The measured pH of 2.0 M $LiNO_3$, 1.7 M $NaNO_3$, 1.6 M NH_4NO_3, and 1.0 M $Mg(NO_3)_2$ ranged between 5 and 7. All salt solutions were shown to be free of organic impurities as revealed by VSFG spectra obtained in the surfactant CH stretching region (2800−3000 cm^{-1}) (Supporting Information). All solutions were thermally equilibrated at room temperature (23 ± 1 °C) over 24 h before use.

Most of the nitrate salts used here were of ACS reagent grade (>98%). This choice was based on the fact that ultrahigh-purity salts (on the basis of higher trace metal purity) typically reveal greater organic contamination and its effect on the VSFG water spectra in the OH stretching region can vary depending on the amount present. In addition, previous VSFG spectra from carbonate, sulfate, and chloride salt solutions demonstrated that for the same chemical species ultrapure (>99.99%) versus high purity (~99%) grade salts display highly similar conventional VSFG and HD-VSFG spectra in the OH region after appropriate pretreatment of salts and salt solutions.[56]

Methods. Conventional and Heterodyne-Detected VSFG Spectroscopy. Conventional VSFG spectroscopy

dx.doi.org/10.1021/jp505770t | J. Phys. Chem. C 2014, 118, 24941−24949

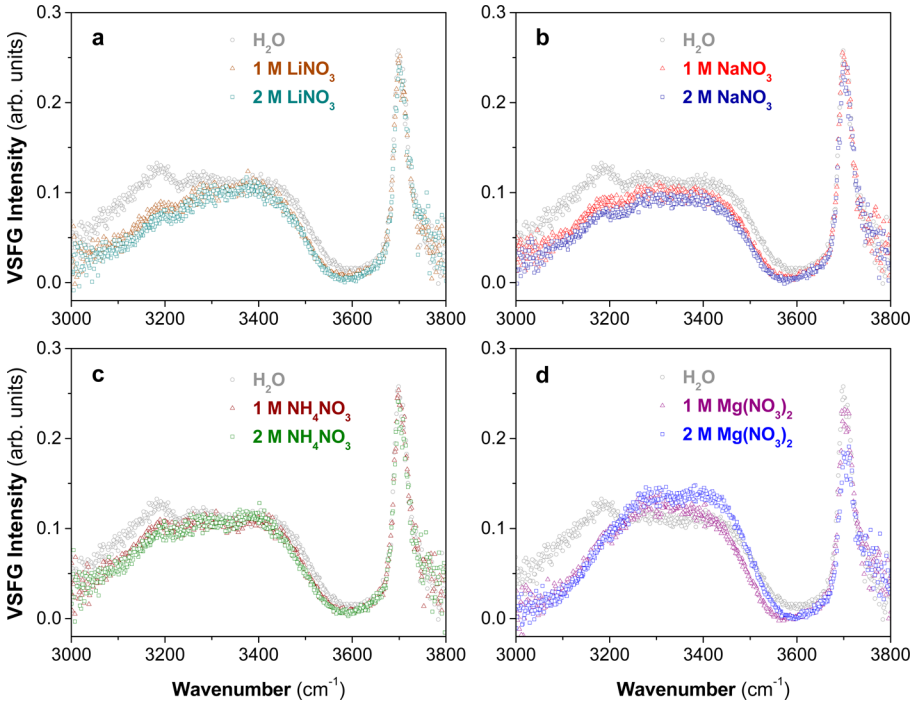

Figure 1. VSFG spectra of air/aqueous interfaces of 1 and 2 M (a) $LiNO_3$, (b) $NaNO_3$, (c) NH_4NO_3, and (d) $Mg(NO_3)_2$ salt solutions over the entire OH stretching region (3000−3800 cm^{-1}). The VSFG spectrum of the neat air/water interface is also shown as reference. The VSFG spectra contain the contributions from the real (Re $\chi_s^{(2)}(\omega_{IR})$) and imaginary (Im $\chi_s^{(2)}(\omega_{IR})$) spectra. Colors of data plotted here will be followed in all subsequent figures.

measurements were performed on a broad-bandwidth VSFG spectrometer setup that has been described elsewhere.[57−59] The HD-VSFG setup adopted here differs from the VSFG one only in the optical configuration of the sample stage area whose design is similar to that reported by Tahara and co-workers.[60−62] The HD-VSFG setup and the data processing procedure used have also been described previously.[63−66] Incident angles for the visible (0.8 μm) and infrared (2.6−3.3 μm in the water OH stretching region) were 59/63 ± 1° and 50/60 ± 1° for the VSFG and HD-VSFG experiments, respectively. The *ssp* (*s* for sum-frequency, *s* for visible, and *p* for infrared) polarization configuration was chosen, and the average incident energy of the visible and infrared beams impinging on the aqueous surface was 300/10 and 260/8 μJ for VSFG and HD-VSFG measurements, respectively. The background-subtracted VSFG spectra of the different air/aqueous solution interfaces were normalized against a nonresonant VSFG spectrum from a GaAs(110) crystal (Lambda Precision Optics) to eliminate the spectral distortion caused by the uneven infrared beam energy distribution at different frequency in the spectral region of interest. In the case of HD-VSFG spectra, the normalization was done against a reference *z*-cut quartz crystal (MTI Corporation).

Neat water spectra were used as a reference for salt comparison to assess reproducibility during the entire experimental period. The reproducibility for both VSFG and HD-VSFG (Im $\chi_s^{(2)}(\omega_{IR})$) spectra of neat water was tested and can be found in the Supporting Information. Im $\chi_s^{(2)}(\omega_{IR})$ spectra of air/aqueous salt solution interfaces were compared to that of neat water such that the interpretation given here is based on the *relative* spectral difference between neat water and the salt solutions. The consistency and trend of these spectra were checked against the deduced VSFG power spectrum ($|\chi_{eff}^{(2)}(\omega_{IR})|^2$) of each nitrate salt solution (Supporting Information) to those measured directly by VSFG spectroscopy. Note that a strict comparison would require taking into account normalization and Fresnel factors correction procedures.[67,68] However, even without these corrections the general trend between salt solutions observed in the VSFG spectra is essentially consistent with the reconstructed power spectra. Only every second and fourth data points are plotted in the conventional VSFG and HD-VSFG spectra, respectively, to avoid spectral clutter.

RESULTS AND DISCUSSION

Influence of Salts on VSFG Spectra. VSFG spectra of the interfacial region of $LiNO_3$, $NaNO_3$, NH_4NO_3, and $Mg(NO_3)_2$ aqueous salt solutions together with that of the neat air/water interface are shown in Figure 1. The interfacial region refers hereafter to the region where concentration gradients exist and which lacks inversion symmetry, hence SFG-active. Only in the case of neat water, the observed VSFG signal mainly originates from the topmost layers (∼1−2), whereas the adjacent sublayers make little contribution. The VSFG spectrum of the neat air/water interface consists of a broad region spanning from 3000 to 3600 cm^{-1} associated with coordinated water molecules with a broad continuum of hydrogen bond lengths and geometries and a narrow band at ∼3700 cm^{-1} assigned to the distinct dangling OH bond of water molecules located in the topmost layer. It is generally accepted that the lower frequency part of the broad region corresponds to water molecules that are highly coordinated with strong hydrogen bonds, and as one moves to higher frequency, water molecules become less coordinated and the hydrogen bonding strength weakens significantly. Other assignments to this broad region have also been proposed.[69−78] The distribution of ions in the interfacial region generates an interfacial electric field induced by the formation of an ionic double layer consisting of sublayers of anions and cations, which extends the region of noncentrosymmetry.[53] The presence of ions can influence the VSFG water signal either by varying (i) the

dx.doi.org/10.1021/jp505770t | J. Phys. Chem. C 2014, 118, 24941−24949

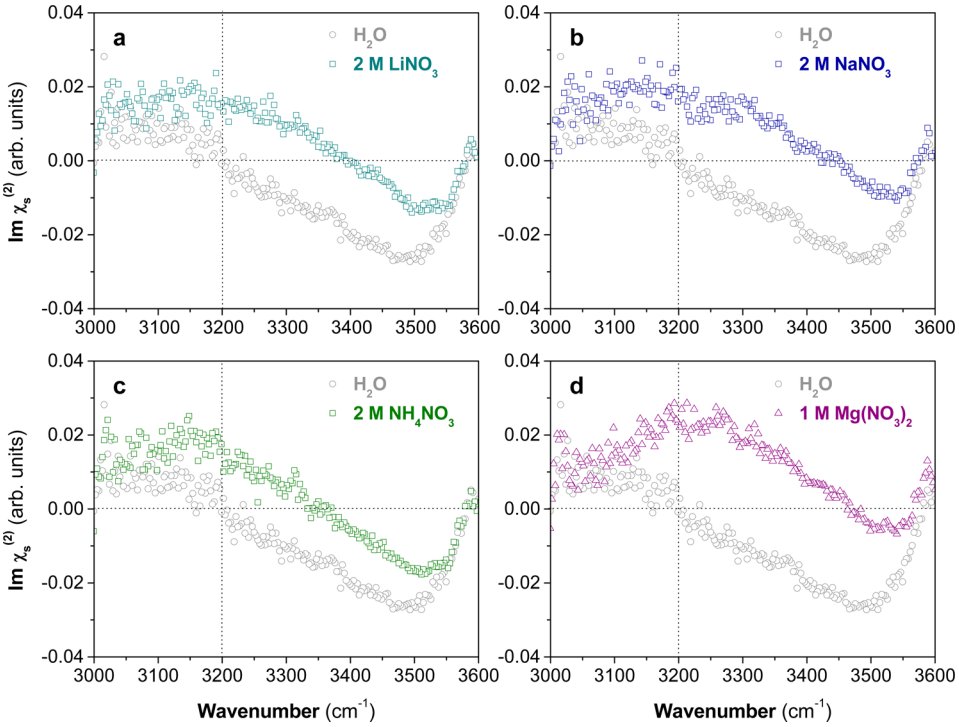

Figure 2. Im $\chi_s^{(2)}(\omega_{IR})$ spectra of air/aqueous interfaces of (a) 2 M $LiNO_3$, (b) 2 M $NaNO_3$, (c) 2 M NH_4NO_3, and (d) 1 M $Mg(NO_3)_2$ salt solutions over the 3000−3600 cm^{-1} spectral region. Im $\chi_s^{(2)}(\omega_{IR})$ spectrum of the neat air/water interface is also shown as reference.

number of contributing water molecules, or (ii) their orientation, and/or (iii) the magnitude of their OH transition dipole moments.

As shown in Figure 1, the addition of nitrate salts to water has a perturbative effect on the interfacial hydrogen-bonding network, the extent of which depends on salt concentration and cation identity. The VSFG spectra of $LiNO_3$, $NaNO_3$, and NH_4NO_3 solutions show an uneven decrease in intensity in the broad OH-bonded water region from 3000 to 3600 cm^{-1} relative to neat water, particularly below 3200 cm^{-1} (Figure 1a−c); however, NH_4NO_3 has the least effect over the entire water stretching region. In contrast, $Mg(NO_3)_2$ induces marked spectral changes: in addition to the intensity decrease at lower frequencies, the broad continuum OH stretching region is enhanced from ∼3250 to 3500 cm^{-1} (Figure 1d). Note here that any pH effect can be ruled out since the pHs of all nitrate solutions fall in the range of 5−7, such that the concentration of hydronium (H_3O^+) ions, which are known to be disruptive to the hydrogen-bonding network and dangling OH,[79] remains quite low. Therefore, the pH of nitrate solutions should only play a minor role in the overall spectral change.

The changes observed in the broad OH stretching continuum region in the VSFG spectra of all nitrate salt solutions point to a weakening of the overall hydrogen-bonding network caused by the interfacial distributions of the countercations and NO_3^-. Note however that the intensity enhancement in the $Mg(NO_3)_2$ spectra at 3300 cm^{-1} could also be due to spectral convolution effects between real and imaginary $\chi_s^{(2)}(\omega_{IR})$ components of the VSFG spectra as was demonstrated for $CaCl_2$ solutions with HD-VSFG spectroscopy.[63] In order to delineate these effects, it becomes advantageous to utilize HD-VSFG spectroscopy (see below).

MD simulated density profiles of low concentrated (≤2 M) $NaNO_3$ solutions showed that NO_3^- has only a weak surface propensity and can mostly be found below the first few water layers but above their Na^+ countercations, which are typically repelled further from the surface primarily through image charge effects.[43] This electrostatic repulsion becomes the dominant force for the Na^+ cations as the absence of NO_3^- surface enhancement weakens any localized electroneutrality effect that would bring them closer to the surface—more so for the case of $Mg(NO_3)_2$ solutions, with highly charged Mg^{2+} cations being repelled deeper in the interfacial region.[44]

In addition to changes in the broad OH region, the intensity of the dangling OH peak drops significantly relative to neat water in the presence of $Mg(NO_3)_2$, whereas no appreciable differences are observed for the other monovalent nitrate solutions. Schnitzer et al. observed a decrease in intensity of the dangling OH peak for ∼0.6 M $NaNO_3$ solutions which became more significant as the salt concentration was increased up to saturation.[54] It was suggested that the perturbation of dangling OH groups on $NaNO_3$ salt solutions is a function of ionic strength, ion pairing, and anion charge density. Prior studies by Allen and co-workers using highly concentrated (∼5 M) NaCl and $MgCl_2$ solutions observed a drop in the dangling OH intensity.[53,80] Yet, in the case of $Mg(NO_3)_2$ solution, intensity decrease was detectable even at the lowest concentration (Figure 1d).

Because the VSFG intensity depends on the number density of oriented water molecules and/or on the alignment of their dipole moments along the surface normal, one or both of these factors could be responsible for the dangling OH peak reduction. For example, MD simulations of $NaNO_3$ solutions predicted a decrease in the dangling OH population as well as a reorientation of subsurface water molecules but only in the high salt concentration regime (>5 M).[43] In contrast, VSFG orientational analysis considered the 3700 cm^{-1} peak decrease from $Mg(NO_3)_2$ solutions to be mainly due to a reorientation of the dangling OH moiety,[27] although this interpretation has been contested on the neat water interface where dangling OH bonds

dx.doi.org/10.1021/jp505770t | J. Phys. Chem. C 2014, 118, 24941−24949

are limited to a narrow range of orientational motion.[81] Yet here we show and confirm unique behavior for Mg^{2+} and additionally found that NH_4^+ does not alter the topmost layer.

Salt-Induced Interfacial Electric Field. The Im $\chi_s^{(2)}(\omega_{IR})$ spectra of the air/aqueous interfaces of $LiNO_3$, $NaNO_3$, NH_4NO_3, and $Mg(NO_3)_2$ salt solutions in the OH stretching region are shown in Figure 2. A decisive advantage of HD-VSFG spectroscopy over its conventional counterpart is that it can directly provide the sign and, in turn, the net orientation of transition dipole moments of SFG-active OH vibrational stretching modes; the positive or negative magnitude of the Im $\chi_s^{(2)}(\omega_{IR})$ water spectrum reveals the direction of the O → H dipole moment, i.e., either toward or away from the vapor phase, respectively. The Im $\chi_s^{(2)}(\omega_{IR})$ spectrum of the neat air/water interface in the OH stretching region is also shown in Figure 2 and is consistent with those of Shen and co-workers and Tahara and co-workers.[61,79,82] It consists of a positive band in the 3000−3200 cm^{-1} region and a broad negative band from 3200 to 3600 cm^{-1}; although the latter region has been explicitly attributed to OH stretch net transition dipole moments oriented preferentially toward the bulk solution, the assignment of the former region continues to be debated.[71,72,75,82] Here we focus on the range above 3200 cm^{-1}.

Similarly to the perturbation observed in the VSFG spectra (Figure 1), the partitioning of NO_3^- and its countercations in the interfacial region also leads to significant spectral changes in the corresponding Im $\chi_s^{(2)}(\omega_{IR})$ spectra of Figure 2, seen in the form of a positive signal enhancement relative to neat water over most of the OH stretching region (up to 3550 cm^{-1}). The Im $\chi_s^{(2)}(\omega_{IR})$ spectrum of the $NaNO_3$ solution presented here (Figure 2b) is consistent with the one previously reported by Tian et al.,[18] although shown here for the first time are the Im $\chi_s^{(2)}(\omega_{IR})$ spectra of $LiNO_3$, NH_4NO_3, and $Mg(NO_3)_2$ solutions. The extent of Im $\chi_s^{(2)}(\omega_{IR})$ spectral intensity is dependent on the cation identity.

The overall enhancement observed for all nitrate solutions from 3200 to 3500 cm^{-1} is related to the reorganization of interfacial water molecules with their net transition dipole moment oriented more toward the gas phase, which is attributed to the generation of a positive interfacial electric field (by convention, the field lines direction is defined from the positive to the negative charge distribution) induced by the ionic double layer formed between NO_3^- anions and countercations. The simplest molecular picture inferred from the Im $\chi_s^{(2)}(\omega_{IR})$ spectra have the NO_3^- anions located predominantly above their countercations.[43,44] The relative position of the ion distributions and, in turn, the direction (positive sign) of the electric field are consistent with the negative surface potential values (because of the relation $\Delta V = -\int E(z)\, dz$) measured on aqueous nitrate solutions.[83,84]

By looking closely at Figure 2, one notices that the intensity of the Im $\chi_s^{(2)}(\omega_{IR})$ spectra and, consequently, the magnitude of the interfacial electric field display a weak but definite cation dependency. (For 1 M nitrate solutions, a cation effect is more difficult to distinguish with Na^+ having only a slightly larger signal intensity than Li^+ and NH_4^+, which are comparable (data not shown).) Such an effect is readily observable with NH_4^+ and Mg^{2+} having respectively the weakest and strongest impact on interfacial water organization (Figure 2c,d), consistent with Figure 1. This cation-specific effect caused by the different NO_3^-/cation distributions can be made more apparent in the Im $\chi_s^{(2)}(\omega_{IR})$ difference spectra taken with respect to neat water (Figure 3). Based on their impact on the reorganization of the

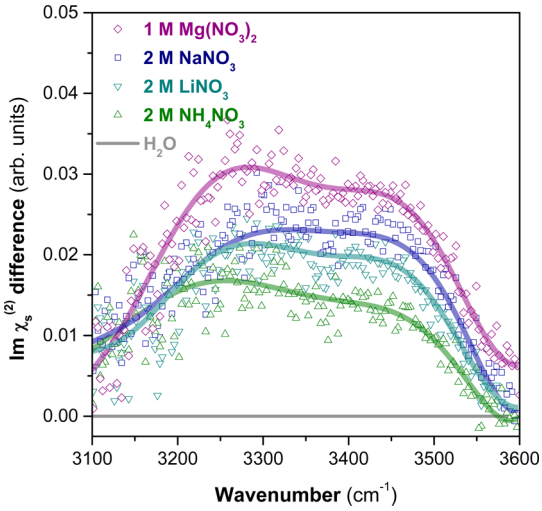

Figure 3. Im $\chi_s^{(2)}(\omega_{IR})$ difference spectra relative to neat water of the ~2 M aqueous nitrate salt solutions. The solid curves serve as eye guides to show the trend in the data.

interfacial water network and, subsequently, on the magnitude of their respective induced electric field, cations can be ranked in the following order: $Mg^{2+} > Na^+ > Li^+ > NH_4^+$.

With the exception of Na^+ and Li^+ ions, the trend follows the decrease of the cation surface charge density and is partially in agreement with available surface potential measurements by Frumkin ($Li^+ > Na^+ > NH_4^+$),[83] and Jarvis and Scheiman ($Mg^{2+} > Na^+$)[84] at the same concentration, although such data remain scarce, insufficiently reproduced, and somewhat dated. Generally speaking, the magnitude of the interfacial electric field depends on the different ion density profiles, i.e., on the overall ion concentration and on the accumulation/depletion and surface propensity of one ionic species relative to another as well as on the spatial separation between peak densities of each ion distribution. NO_3^- anions display a greater surface propensity than its countercation, thereby forming an ionic double layer structure with a resulting positive electric field. The Im $\chi_s^{(2)}(\omega_{IR})$ spectrum in Figure 2b would also suggest that the magnitude of this field is strong enough to reorient the OH dipole moments of a majority of water species, with the exception of those contributing to the spectral region from 3450 to 3550 cm^{-1}. However, this observation remains difficult to explain with the MD simulations that predicted quasi-overlapping ion density profiles for NO_3^- and Na^+ over most of the interfacial region. Interestingly, Im $\chi_s^{(2)}(\omega_{IR})$ spectra of $LiNO_3$ and $NaNO_3$ are very similar (Figure 2a,b). This is counterintuitive because Li^+ cations, with their higher surface charge density, should in principle be repelled deeper in the interfacial region relative to Na^+ due to greater image charge interactions. This was recently reported in the Im $\chi_s^{(2)}(\omega_{IR})$ spectra of chloride salt solutions.[85]

The peculiar surface propensity of Li^+ ions could be due to the presence of two strongly bound hydration shells compared to Na^+ ions,[86] which would make them larger and, possibly, more effective at screening their surface charge. This is consistent with IR spectroscopy results by Lisy and co-workers which also showed the reversal of Na^+ and Li^+ in the frequency shift of the OH stretching mode observed for a series of alkali ion water clusters (n = 4, 5).[87] MD simulations of the surface tension increment of air/aqueous interfaces of alkali chloride solutions have also shown that Li^+ ions are less repelled from the interface than larger Na^+ ions.[88] This has been rationalized by the strong

dx.doi.org/10.1021/jp505770t | J. Phys. Chem. C 2014, 118, 24941−24949

binding of the Li^+ first water solvation shell, making Li^+ appear larger. In other words, in the case of Li^+ ions with their two hydration shells, the free energy cost associated with solvating a larger ionic cavity combined with repulsive electrostatic interactions could slightly increase their surface propensity relative to Na^+ cations.

As mentioned above, NH_4NO_3 solutions have an influence on the orientation of interfacial water molecules. Here, the weakness of the E-field as shown from the Im $\chi_s^{(2)}(\omega_{IR})$ spectrum (Figure 2c) suggests that NH_4^+ cations reside closer to NO_3^- than the alkali cations. It is well-known that in bulk dilute aqueous NH_4NO_3 solutions the perturbation of NH_4^+ on nitrates is negligible because NH_4^+ ions form hydrogen bonds with similar strength as water.[89] Even though there is currently no MD simulations of the air/NH_4NO_3 solution interface, one can gain insight from the Im $\chi_s^{(2)}(\omega_{IR})$ spectra and MD simulations of NaCl and NH_4Cl salt solutions, which showed NH_4^+ cations closer by about 1 Å to the topmost surface layer than Na^+.[26] The NH_4Cl distribution could not be explained simply in terms of anion−cation interactions; it was later hypothesized in another study that the structured layer of Cl^- ions may result in an ordered water layer that would interact directly with NH_4^+ through dipolar and hydrogen-bonding interactions.[90] A similar mechanism might be helpful for understanding the NH_4^+/NO_3^- distribution. Note that this would also be in line with the surface-bulk partitioning model of Pegram and Record.[91,92] According to this model, the partitioning of cations, based on the ratio of their surface to bulk concentrations, is predicted to follow the trend $NH_4^+ > Na^+ \approx Li^+$. Interestingly, the value for the partition coefficient of Li^+, albeit with a large uncertainty, is almost identical to that of Na^+.

In contrast, among all the nitrate salt solutions studied in this work, the Im $\chi_s^{(2)}(\omega_{IR})$ spectrum of 1 M $Mg(NO_3)_2$ shows the largest positive enhancement relative to water (Figure 3). The difference spectrum reveals that $Mg(NO_3)_2$ more strongly reorganizes and orients interfacial water molecules and gives rise to a larger electric field relative to any other nitrate salts. The larger electric field enhancement of $Mg(NO_3)_2$ compared to other nitrate solutions (at similar NO_3^- concentrations) suggests that the induced net electric field may originate from a greater charge separation between the Mg^{2+} and NO_3^- distributions. Indeed, because of its higher surface charge density, Mg^{2+} may be repelled deeper in the interfacial region compared to monovalent cations to reduce the electrostatic penalty of image charge effects. Although this scenario is physically sound, it is oversimplified as MD simulations of air−aqueous salt interface of $Mg(NO_3)_2$ have shown that Mg^{2+} and NO_3^- are distributed in a complex multilayer-like structure,[44] much like the one predicted for $MgCl_2$ solutions.[93]

At present, our interpretation of the observed electric field enhancement may be oversimplified in that a single ionic double layer is suggested for the monovalent cation−NO_3^- salts. Clearly multilayers could exist, and there is MD simulation evidence that Mg^{2+} gives rise to such behavior, thus strongly suggesting complexity arises for divalent cations of NO_3^- salts. In all cases, an increase in interfacial depth[24,94] is expected, i.e., an increase in the SFG-active region,[95] which can also be explained in a $\chi^{(3)}$ model.[96]

Implications for Atmospheric Chemistry and Thundercloud Electrification. NH_4^+, Mg^{2+}, and Na^+ along with NO_3^- are commonly found in atmospheric aerosols, sea ice, and snowpacks through heterogeneous reactions and direct deposition.[2,97−100] And, it is also known that both the kinetics and mechanisms of interfacial reactions are different from those in the isotropic bulk phase.[1,101−103] Hence, a reversed and/or increased surface electric field, in addition to the presence of NO_3^- anions near the surface of aqueous aerosols, will impact interfacial reactions and thus the associated kinetics. For example, noting that photolysis rates of NO_3^- ions in the polar snowpack in the absence of bromide and chloride ions are underestimated,[11] enhanced photochemistry with production of NO_x and OH radicals will increase the oxidizing capacity of the atmosphere.

Additionally, although NO_3^- exists in the interfacial region, countercations such as NH_4^+ are not completely absent from the interface. They do not show a strong surface preference, but a small population still likely exists. Moreover, the interfacial electric field generated from the ionic double layer(s), in all cases studied here, is larger than that observed on neat water and thus likely plays a role in the electrostatics of adsorption of molecules from the gas phase.

Furthermore, the importance of including chemical composition effects of aerosol in atmospheric models is currently understated. In current global modeling studies, ammonium and nitrate are excluded as factors in the direct aerosol radiative forcing,[34,104] even though they have been identified as significant anthropogenic sources of the aerosol load;[105] the rapid increases in nitrogen emissions may be capable of generating enough nitrate aerosols to offset the expected decline in sulfate forcing.[105] Thus, a more complete description of aerosol composition including hygroscopic components like NO_3^- and NH_4^+ is warranted in global atmospheric models.

Finally, the surface propensity of all ionic species including NH_4^+, Mg^{2+}, and Na^+, and NO_3^- sheds light on charge transfer in thundercloud electrification processes. It is found in a large range of observations that enhanced positive lightning is associated with smoke, rich in nitrates and chlorides, yet the origin of this phenomenon is not fully understood. Ions such as NO_3^-, residing closer to the surface of the larger falling ice particles in thunderclouds (graupels), could be preferentially transferred to the quasi-liquid interfacial layer of the small rising ice crystals during collisions between ice crystals and graupels, resulting in the positive charging of the falling graupels.[14]

■ CONCLUSIONS

We show that the cations NH_4^+, Na^+, Mg^{2+}, and Li^+ have a significant impact on the surface electric field when studied with NO_3^- and that nitrate ions have a distribution that is above its countercation distribution at the air−aqueous interface. Thus, NH_4^+, Na^+, Mg^{2+}, and Li^+ along with NO_3^- create an ionic double layer structure that generates a positive electric field whose magnitude also depends on the cation identity. The impact of the cations on the magnitude of the induced electric field can be ranked in the order $Mg^{2+} > Na^+ > Li^+ > NH_4^+$, generally consistent with the order of their respective surface charge density with the exception of Na^+ and Li^+ ions. It is noteworthy that, in comparison to alkali cations, NH_4^+ cations would be located closer to NO_3^- in this double layer structure, even though NH_4^+ typically exhibits only weak interactions with NO_3^- in NH_4NO_3 bulk aqueous solutions. In addition, depending on the cation, interfacial ion distributions cause a full reversal in the surface electric field, which in turn causes the reorientation of the OH transition dipole moments of water species. This observed phenomenon impacts surface processes including adsorption, chemistry, and atmospheric aerosol aging as well as has implications for understanding of thundercloud electrification.

dx.doi.org/10.1021/jp505770t | J. Phys. Chem. C 2014, 118, 24941−24949

■ ASSOCIATED CONTENT

Supporting Information

Raman calibration curves of NH_4NO_3 solution; conventional VSFG and HD-VSFG (Im $\chi_s^{(2)}(\omega_{IR})$) spectra of neat water obtained through the entire experimental period demonstrating system and phase stability; VSFG power spectra ($|\chi_{eff}^{(2)}(\omega_{IR})|^2$) and Re $\chi_s^{(2)}(\omega_{IR})$ spectra deduced from the air/aqueous interface of nitrate salt solution interfaces; VSFG spectra of neat water and nitrate salt solutions in the surfactant CH stretching region (2800−3000 cm^{-1}). This material is available free of charge via the Internet at http://pubs.acs.org.

■ AUTHOR INFORMATION

Corresponding Author

*Tel +1-614-292-4707; Fax +1-614-292-1685; e-mail allen@chemistry.ohio-state.edu (H.C.A.).

Notes

The authors declare no competing financial interest.

■ ACKNOWLEDGMENTS

The authors acknowledge the financial support of NSF (CHE-1111762) and the DOE-BES (DE-FG02-04ER15495). We are grateful to Drs. James Lisy and Karen Callahan for helpful discussions. We also acknowledge Ellen Adams for sample preparation. W. H. acknowledges a Presidential Fellowship from The Ohio State University.

■ REFERENCES

(1) Knipping, E. M.; Lakin, M. J.; Foster, K. L.; Jungwirth, P.; Tobias, D. J.; Gerber, R. B.; Dabdub, D.; Finlayson-Pitts, B. J. Experiments and Simulations of Ion-Enhanced Interfacial Chemistry on Aqueous NaCl Aerosols. *Science* **2000**, *288*, 301−306.

(2) Finlayson-Pitts, B. J.; Pitts Jr., J. N. *Chemistry of the Upper and Lower Atmosphere: Theory, Experiments and Applications*; Academic Press: San Diego, CA, 2000.

(3) Finlayson-Pitts, B. J. The Tropospheric Chemistry of Sea Salt: A Molecular-Level View of the Chemistry of NaCl and NaBr. *Chem. Rev.* **2003**, *103*, 4801−4822.

(4) Donaldson, D. J.; Valsaraj, K. T. Adsorption and Reaction of Trace Gas-Phase Organic Compounds on Atmospheric Water Film Surfaces: A Critical Review. *Environ. Sci. Technol.* **2010**, *44*, 865−873.

(5) Finlayson-Pitts, B. J. Reactions at Surfaces in the Atmosphere: Integration of Experiments and Theory as Necessary (But Not Necessarily Sufficient) for Predicting the Physical Chemistry of Aerosols. *Phys. Chem. Chem. Phys.* **2009**, *11*, 7760−7779.

(6) Gopalakrishnan, S.; Liu, D. F.; Allen, H. C.; Kuo, M.; Shultz, M. J. Vibrational Spectroscopic Studies of Aqueous Interfaces: Salts, Acids, Bases, and Nanodrops. *Chem. Rev.* **2006**, *106*, 1155−1175.

(7) Jungwirth, P.; Finlayson-Pitts, B. J.; Tobias, D. J. Introduction: Structure and Chemistry at Aqueous Interfaces. *Chem. Rev.* **2006**, *106*, 1137−1139.

(8) Laß, K.; Kleber, J.; Friedrichs, G. Vibrational Sum-Frequency Generation as a Probe for Composition, Chemical Reactivity, and Film Formation Dynamics of the Sea Surface Nanolayer. *Limnol. Oceanogr.: Methods* **2010**, *8*, 216−228.

(9) Logan, C. A. A Review of Ocean Acidification and America's Response. *Bioscience* **2010**, *60*, 819−828.

(10) Finlayson-Pitts, B. J.; Wingen, L. M.; Sumner, A. L.; Syomin, D.; Ramazan, K. A. The Heterogeneous Hydrolysis of NO_2 in Laboratory Systems and in Outdoor and Indoor Atmospheres: An Integrated Mechanism. *Phys. Chem. Chem. Phys.* **2003**, *5*, 223−242.

(11) Richards, N. K.; Wingen, L. M.; Callahan, K. M.; Nishino, N.; Kleinman, M. T.; Tobias, D. J.; Finlayson-Pitts, B. J. Nitrate Ion Photolysis in Thin Water Films in the Presence of Bromide Ions. *J. Phys. Chem. A* **2011**, *115*, 5810−5821.

(12) Boxe, C. S.; Colussi, A. J.; Hoffmann, M. R.; Perez, I. M.; Murphy, J. G.; Cohen, R. C. Kinetics of NO and NO_2 Evolution from Illuminated Frozen Nitrate Solutions. *J. Phys. Chem. A* **2006**, *110*, 3578−3583.

(13) Dominé, F.; Shepson, P. B. Air-Snow Interactions and Atmospheric Chemistry. *Science* **2002**, *297*, 1506−1510.

(14) Jungwirth, P.; Rosenfeld, D.; Buch, V. A Possible New Molecular Mechanism of Thundercloud Electrification. *Atmos. Res.* **2005**, *76*, 190−205.

(15) Sparks, D. L. Toxic Metals in the Environment: The Role of Surfaces. *Elements* **2005**, *1*, 193−197.

(16) Lassin, A.; Azaroual, M.; Mercury, L. Geochemistry of Unsaturated Soil Systems: Aqueous Speciation and Solubility of Minerals and Gases in Capillary Solutions. *Geochim. Cosmochim. Acta* **2005**, *69*, 5187−5201.

(17) Pettenati, M.; Mercury, L.; Azaroual, M. Capillary Geochemistry in Non-Saturated Zone of Soils. Water Content and Geochemical Signatures. *Appl. Geochem.* **2008**, *23*, 3799−3818.

(18) Tian, C. S.; Byrnes, S. J.; Han, H. L.; Shen, Y. R. Surface Propensities of Atmospherically Relevant Ions in Salt Solutions Revealed by Phase-Sensitive Sum Frequency Vibrational Spectroscopy. *J. Phys. Chem. Lett.* **2011**, *2*, 1946−1949.

(19) Lihavainen, H.; Kerminen, V. M.; Komppula, M.; Hyvarinen, A. P.; Laakia, J.; Saarikoski, S.; Makkonen, U.; Kivekas, N.; Hillamo, R.; Kulmala, M.; et al. Measurements of the Relation between Aerosol Properties and Microphysics and Chemistry of Low Level Liquid Water Clouds in Northern Finland. *Atmos. Chem. Phys.* **2008**, *8*, 6925−6938.

(20) Talbot, R. W.; Dibb, J. E.; Loomis, M. B. Influence of Vertical Transport on Free Tropospheric Aerosols over the Central USA in Springtime. *Geophys. Res. Lett.* **1998**, *25*, 1367−1370.

(21) Millero, F. J. *Chemical Oceanography*, 3rd ed.; CRC Press: Boca Raton, FL, 2005.

(22) Jungwirth, P.; Tobias, D. J. Specific Ion Effects at the Air/Water Interface. *Chem. Rev.* **2006**, *106*, 1259−1281.

(23) Jungwirth, P.; Tobias, D. J. Molecular Structure of Salt Solutions: A New View of the Interface with Implications for Heterogeneous Atmospheric Chemistry. *J. Phys. Chem. B* **2001**, *105*, 10468−10472.

(24) Liu, D.; Ma, G.; Levering, L. M.; Allen, H. C. Vibrational Spectroscopy of Aqueous Sodium Halide Solutions and Air-Liquid Interfaces: Observation of Increased Interfacial Depth. *J. Phys. Chem. B* **2004**, *108*, 2252−2260.

(25) Bush, M. F.; O'Brien, J. T.; Prell, J. S.; Wu, C.-C.; Saykally, R. J.; Williams, E. R. Hydration of Alkaline Earth Metal Dications: Effects of Metal Ion Size Determined Using Infrared Action Spectroscopy. *J. Am. Chem. Soc.* **2009**, *131*, 13270−13277.

(26) Gopalakrishnan, S.; Jungwirth, P.; Tobias, D. J.; Allen, H. C. Air-Liquid Interfaces of Aqueous Solution Containing Ammonium and Sulfate: Spectroscopic and Molecular Dynamics Studies. *J. Phys. Chem. B* **2005**, *109*, 8861−8872.

(27) Xu, M.; Spinney, R.; Allen, H. C. Water Structure at the Air-Aqueous Interface of Divalent Cation and Nitrate Solutions. *J. Phys. Chem. B* **2009**, *113*, 4102−4110.

(28) Du, H.; Rasaiah, J. C.; Miller, J. D. Structural and Dynamic Properties of Concentrated Alkali Halide Solutions: A Molecular Dynamics Simulation Study. *J. Phys. Chem. B* **2007**, *111*, 209−217.

(29) Bian, H. T.; Feng, R. R.; Guo, Y.; Wang, H. F. Specific Na^+ and K^+ Cation Effects on the Interfacial Water Molecules at the Air/Aqueous Salt Solution Interfaces Probed with Nonresonant Second Harmonic Generation. *J. Chem. Phys.* **2009**, *130*, 134709/1−134709/11.

(30) Feng, R.-r.; Bian, H.-t.; Guo, Y.; Wang, H.-f. Spectroscopic Evidence for the Specific Na^+ and K^+ Interactions with the Hydrogen-Bonded Water Molecules at the Electrolyte Aqueous Solution Surfaces. *J. Chem. Phys.* **2009**, *130*, 134710/1−134710/6.

(31) Finlayson-Pitts, B. J.; Hemminger, J. C. Physical Chemistry of Airborne Sea Salt Particles and Their Components. *J. Phys. Chem. A* **2000**, *104*, 11463−11477.

(32) Orel, A. E.; Seinfeld, J. H. Nitrate Formation in Atmospheric Aerosols. *Environ. Sci. Technol.* **1977**, *11*, 1000−1007.

(33) Hildemann, L. M.; Russell, A. G.; Cass, G. R. Ammonia and Nitric Acid - Acid Concentrations in Equilibrium with Atmospheric Aerosols - Experiment vs Theory. *Atmos. Environ.* **1984**, *18*, 1737−1750.
(34) Bauer, S. E.; Koch, D.; Unger, N.; Metzger, S. M.; Shindell, D. T.; Streets, D. G. Nitrate Aerosols Today and in 2030: A Global Simulation Including Aerosols and Troposphere Ozone. *Atmos. Chem. Phys.* **2007**, *7*, 5043−5059.
(35) Gibson, E. R.; Hudson, P. K.; Grassian, V. H. Physicochemical Properties of Nitrate Aerosols: Implications for the Atmosphere. *J. Phys. Chem. A* **2006**, *110*, 11785−11799.
(36) Chu, L.; Anastasio, C. Quantum Yields of Hydroxyl Radical and Nitrogen Dioxide from the Photolysis of Nitrate on Ice. *J. Phys. Chem. A* **2003**, *107*, 9594−9602.
(37) Honrath, R. E.; Guo, S.; Peterson, M. C.; Dziobak, M. P.; Dibb, J. E.; Arsenault, M. A. Photochemical Production of Gas Phase NO_x from Ice Crystal NO_3. *J. Geophys. Res.: Atmos.* **2000**, *105*, 24183−24190.
(38) Honrath, R. E.; Peterson, M. C.; Dziobak, M. P.; Dibb, J. E.; Arsenault, M. A.; Green, S. A. Release of NO_x from Sunlight-Irradiated Midlatitude Snow. *Geophys. Res. Lett.* **2000**, *27*, 2237−2240.
(39) Mack, J.; Bolton, J. R. Photochemistry of Nitrite and Nitrate in Aqueous Solution: A Review. *J. Photochem. Photobiol., A* **1999**, *128*, 1−13.
(40) Ault, A. P.; Guasco, T. L.; Ryder, O. S.; Baltrusaitis, J.; Cuadra-Rodriguez, L. A.; Collins, D. B.; Ruppel, M. J.; Bertram, T. H.; Prather, K. A.; Grassian, V. H. Inside Versus Outside: Ion Redistribution in Nitric Acid Reacted Sea Spray Aerosol Particles as Determined by Single Particle Analysis. *J. Am. Chem. Soc.* **2013**, *135*, 14528−14531.
(41) Salvador, P.; Curtis, J. E.; Tobias, D. J.; Jungwirth, P. Polarizability of the Nitrate Anion and Its Solvation at the Air/Water Interface. *Phys. Chem. Chem. Phys.* **2003**, *5*, 3752−3757.
(42) Dang, L. X.; Chang, T.-M.; Roeselova, M.; Garrett, B. C.; Tobias, D. J. On NO_3^--H_2O Interactions in Aqueous Solutions and at Interfaces. *J. Chem. Phys.* **2006**, *124*, 066101/1−066101/3.
(43) Thomas, J. L.; Roeselova, M.; Dang, L. X.; Tobias, D. J. Molecular Dynamics Simulations of the Solution-Air Interface of Aqueous Sodium Nitrate. *J. Phys. Chem. A* **2007**, *111*, 3091−3098.
(44) Minofar, B.; Vacha, R.; Wahab, A.; Mahiuddin, S.; Kunz, W.; Jungwirth, P. Propensity for the Air/Water Interface and Ion Pairing in Magnesium Acetate vs Magnesium Nitrate Solutions: Molecular Dynamics Simulations and Surface Tension Measurements. *J. Phys. Chem. B* **2006**, *2006*, 15939−15944.
(45) Cheng, J.; Vecitis, C. D.; Hoffmann, M. R.; Colussi, A. J. Experimental Anion Affinities for the Air/Water Interface. *J. Phys. Chem. B* **2006**, *110*, 25598−25602.
(46) Brown, M. A.; Winter, B.; Faubel, M.; Hemminger, J. C. Spatial Distribution of Nitrate and Nitrite Anions at the Liquid/Vapor Interface of Aqueous Solutions. *J. Am. Chem. Soc.* **2009**, *131*, 8354−8355.
(47) Goebbert, D. J.; Garand, E.; Wende, T.; Bergmann, R.; Meijer, G.; Asmis, K. R.; Neumark, D. M. Infrared Spectroscopy of the Microhydrated Nitrate Ions $NO_3^-(H_2O)_{1-6}$. *J. Phys. Chem. A* **2009**, *113*, 7584−7592.
(48) Wren, S. N.; Donaldson, D. J. Glancing-Angle Raman Study of Nitrate and Nitric Acid at the Air-Aqueous Interface. *Chem. Phys. Lett.* **2012**, *522*, 1−10.
(49) Otten, D. E.; Petersen, P. B.; Saykally, R. J. Observation of Nitrate Ions at the Air/Water Interface by UV-Second Harmonic Generation. *Chem. Phys. Lett.* **2007**, *449*, 261−265.
(50) Richmond, G. L. Molecular Bonding and Interactions at Aqueous Surfaces as Probed by Vibrational Sum Frequency Spectroscopy. *Chem. Rev.* **2002**, *102*, 2693−2724.
(51) Shen, Y. R.; Ostroverkhov, V. Sum-Frequency Vibrational Spectroscopy on Water Interfaces: Polar Orientation of Water Molecules at Interfaces. *Chem. Rev.* **2006**, *106*, 1140−1154.
(52) Shultz, M. J.; Baldelli, S.; Schnitzer, C.; Simonelle, D. Aqueous Solution/Air Interfaces Probed with Sum Frequency Generation Spectroscopy. *J. Phys. Chem. B* **2002**, *106*, 5313−5324.
(53) Allen, H. C.; Casillas-Ituarte, N. N.; Sierra-Hernandez, M. R.; Chen, X. K.; Tang, C. Y. Shedding Light on Water Structure at Air-Aqueous Interfaces: Ions, Lipids, and Hydration. *Phys. Chem. Chem. Phys.* **2009**, *11*, 5538−5549.
(54) Schnitzer, C. S.; Baldelli, S.; Shultz, M. J. Sum Frequency Generation of Water on NaCl, $NaNO_3$, $KHSO_4$, HCl, HNO_3, and H_2SO_4 Aqueous Solutions. *J. Phys. Chem. B* **2000**, *104*, 585−590.
(55) Xu, M.; Tang, C. Y.; Jubb, A. M.; Chen, X. K.; Allen, H. C. Nitrate Anions and Ion Pairing at the Air-Aqueous Interface. *J. Phys. Chem. C* **2009**, *113*, 2082−2087.
(56) Hua, W.; Verreault, D.; Adams, E. M.; Huang, Z. S.; Allen, H. C. Impact of Salt Purity on Interfacial Water Organization Revealed by Conventional and Heterodyne-Detected Vibrational Sum Frequency Generation Spectroscopy. *J. Phys. Chem. C* **2013**, *117*, 19577−19585.
(57) Hommel, E. L.; Allen, H. C. Broadband Sum Frequency Generation with Two Regenerative Amplifiers: Temporal Overlap of Femtosecond and Picosecond Light Pulses. *Anal. Sci.* **2001**, *17*, 137−139.
(58) Ma, G.; Allen, H. C. Surface Studies of Aqueous Methanol Solutions by Vibrational Broad Bandwidth Sum Frequency Generation Spectroscopy. *J. Phys. Chem. B* **2003**, *107*, 6343−6349.
(59) Tang, C. Y.; Allen, H. C. Ionic Binding of Na^+ Versus K^+ to the Carboxylic Acid Headgroup of Palmitic Acid Monolayers Studied by Vibrational Sum Frequency Generation Spectroscopy. *J. Phys. Chem. A* **2009**, *113*, 7383−7393.
(60) Mondal, J. A.; Nihonyanagi, S.; Yamaguchi, S.; Tahara, T. Structure and Orientation of Water at Charged Lipid Monolayer/Water Interfaces Probed by Heterodyne-Detected Vibrational Sum Frequency Generation Spectroscopy. *J. Am. Chem. Soc.* **2010**, *132*, 10656−10657.
(61) Nihonyanagi, S.; Yamaguchi, S.; Tahara, T. Direct Evidence for Orientational Flip-Flop of Water Molecules at Charged Interfaces: A Heterodyne-Detected Vibrational Sum Frequency Generation Study. *J. Chem. Phys.* **2009**, *130*, 204704/1−204704/5.
(62) Nihonyanagi, S.; Yamaguchi, S.; Tahara, T. Water Hydrogen Bond Structure near Highly Charged Interfaces Is Not Like Ice. *J. Am. Chem. Soc.* **2010**, *132*, 6867−6869.
(63) Hua, W.; Jubb, A. M.; Allen, H. C. Electric Field Reversal of Na_2SO_4, $(NH_4)_2SO_4$, and Na_2CO_3 Relative to $CaCl_2$ and NaCl at the Air/Aqueous Interface Revealed by Heterodyne Detected Phase-Sensitive Sum Frequency. *J. Phys. Chem. Lett.* **2011**, *2*, 2515−2520.
(64) Hua, W.; Chen, X. K.; Allen, H. C. Phase-Sensitive Sum Frequency Revealing Accommodation of Bicarbonate Ions, and Charge Separation of Sodium and Carbonate Ions within the Air/Water Interface. *J. Phys. Chem. A* **2011**, *115*, 6233−6238.
(65) Chen, X. K.; Hua, W.; Huang, Z. S.; Allen, H. C. Interfacial Water Structure Associated with Phospholipid Membranes Studied by Phase-Sensitive Vibrational Sum Frequency Generation Spectroscopy. *J. Am. Chem. Soc.* **2010**, *132*, 11336−11342.
(66) Chen, X. K.; Allen, H. C. Water Structure at Aqueous Solution Surfaces of Atmospherically Relevant Dimethyl Sulfoxide and Methanesulfonic Acid Revealed by Phase-Sensitive Sum Frequency Spectroscopy. *J. Phys. Chem. B* **2010**, *114*, 14983−14988.
(67) Feng, R.-r.; Guo, Y.; Lue, R.; Velarde, L.; Wang, H.-f. Consistency in the Sum Frequency Generation Intensity and Phase Vibrational Spectra of the Air/Neat Water Interface. *J. Phys. Chem. A* **2011**, *115*, 6015−6027.
(68) Pool, R. E.; Versluis, J.; Backus, E. H. G.; Bonn, M. Comparative Study of Direct and Phase-Specific Vibrational Sum-Frequency Generation Spectroscopy: Advantages and Limitations. *J. Phys. Chem. B* **2011**, *115*, 15362−15369.
(69) Tian, C. S.; Shen, Y. R. Sum-Frequency Vibrational Spectroscopic Studies of Water/Vapor Interfaces. *Chem. Phys. Lett.* **2009**, *470*, 1−6.
(70) Walker, D. S.; Hore, D. K.; Richmond, G. L. Understanding the Population, Coordination, and Orientation of Water Species Contributing to the Nonlinear Optical Spectroscopy of the Vapor-Water Interface through Molecular Dynamics Simulations. *J. Phys. Chem. B* **2006**, *110*, 20451−20459.
(71) Sovago, M.; Campen, R. K.; Bakker, H. J.; Bonn, M. Hydrogen Bonding Strength of Interfacial Water Determined with Surface Sum-Frequency Generation. *Chem. Phys. Lett.* **2009**, *470*, 7−12.

(72) Ishiyama, T.; Morita, A. Analysis of Anisotropic Local Field in Sum Frequency Generation Spectroscopy with the Charge Response Kernel Water Model. *J. Chem. Phys.* **2009**, *131*, 244714/1−244714/7.
(73) Auer, B. M.; Skinner, J. L. Water: Hydrogen Bonding and Vibrational Spectroscopy, in the Bulk Liquid and at the Liquid/Vapor Interface. *Chem. Phys. Lett.* **2009**, *470*, 13−20.
(74) Fan, Y. B.; Chen, X.; Yang, L. J.; Cremer, P. S.; Gao, Y. Q. On the Structure of Water at the Aqueous/Air Interface. *J. Phys. Chem. B* **2009**, *113*, 11672−11679.
(75) Pieniazek, P. A.; Tainter, C. J.; Skinner, J. L. Surface of Liquid Water: Three-Body Interactions and Vibrational Sum-Frequency Spectroscopy. *J. Am. Chem. Soc.* **2011**, *133*, 10360−10363.
(76) Pieniazek, P. A.; Tainter, C. J.; Skinner, J. L. Interpretation of the Water Surface Vibrational Sum-Frequency Spectrum. *J. Chem. Phys.* **2011**, *135*, 044701/1−044701/12.
(77) Skinner, J. L.; Pieniazek, P. A.; Gruenbaum, S. M. Vibrational Spectroscopy of Water at Interfaces. *Acc. Chem. Res.* **2012**, *45*, 93−100.
(78) Raymond, E. A.; Tarbuck, T. L.; Brown, M. G.; Richmond, G. L. Hydrogen-Bonding Interactions at the Vapor/Water Interface Investigated by Vibrational Sum-Frequency Spectroscopy of HOD/H_2O/D_2O Mixtures and Molecular Dynamics Simulations. *J. Phys. Chem. B* **2003**, *107*, 546−556.
(79) Tian, C. S.; Ji, N.; Waychunas, G. A.; Shen, Y. R. Interfacial Structures of Acidic and Basic Aqueous Solutions. *J. Am. Chem. Soc.* **2008**, *130*, 13033−13039.
(80) Casillas-Ituarte, N. N.; Callahan, K. M.; Tang, C. Y.; Chen, X. K.; Roeselova, M.; Tobias, D. J.; Allen, H. C. Surface Organization of Aqueous $MgCl_2$ and Application to Atmospheric Marine Aerosol Chemistry. *Proc. Natl. Acad. Sci. U. S. A.* **2010**, *107*, 6616−6621.
(81) Gan, W.; Wu, D.; Zhang, Z.; Feng, R. R.; Wang, H. F. Polarization and Experimental Configuration Analyses of Sum Frequency Generation Vibrational Spectra, Structure, and Orientational Motion of the Air/Water Interface. *J. Chem. Phys.* **2006**, *124*, 114705/1−114705/15.
(82) Ji, N.; Ostroverkhov, V.; Tian, C. S.; Shen, Y. R. Characterization of Vibrational Resonances of Water-Vapor Interfaces by Phase-Sensitive Sum-Frequency Spectroscopy. *Phys. Rev. Lett.* **2008**, *100*, 096102/1−096102/4.
(83) Frumkin, A. Phasengrenzekräfte und Adsorption an der Trennungsfläche Luft/Lösung Anorganischer Electrolyte. *Z. Phys. Chem.* **1924**, *109*, 34−48.
(84) Jarvis, N. L.; Scheiman, M. A. Surface Potentials of Aqueous Electrolyte Solutions. *J. Phys. Chem.* **1968**, *72*, 74−78.
(85) Hua, W.; Verreault, D.; Huang, Z.; Adams, E. M.; Allen, H. C. Cation Effects on Interfacial Water Organization of Aqueous Chloride Solutions. I. Monovalent Cations: Li^+, Na^+, K^+, and NH_4^+. *J. Phys. Chem. B* **2014**, *118*, 8433−8440.
(86) Mähler, J.; Persson, I. A Study of the Hydration of the Alkali Metal Ions in Aqueous Solution. *Inorg. Chem.* **2012**, *51*, 425−438.
(87) Miller, D. J.; Lisy, J. M. Entropic Effects on Hydrated Alkali-Metal Cations: Infrared Spectroscopy and Ab Initio Calculations of $M^+(H_2O)_{X=2-5}$ Cluster Ions for M = Li, Na, K, and Cs. *J. Am. Chem. Soc.* **2008**, *130*, 15393−15404.
(88) Horinek, D.; Herz, A.; Vrbka, L.; Sedlmeier, F.; Mamatkulov, S. I.; Netz, R. R. Specific Ion Adsorption at the Air/Water Interface: The Role of Hydrophobic Solvation. *Chem. Phys. Lett.* **2009**, *479*, 173−183.
(89) Xu, M.; Larentzos, J. P.; Roshdy, M.; Criscenti, L. J.; Allen, H. C. Aqueous Divalent Metal-Nitrate Interactions: Hydration Versus Ion Pairing. *Phys. Chem. Chem. Phys.* **2008**, *10*, 4793−4801.
(90) Fu, C. F.; Tian, S. X. Thermodynamics of Ammonia and Ammonium Ion at the Aqueous Solution-Air Interfaces. *J. Phys. Chem. C* **2013**, *117*, 13011−13020.
(91) Pegram, L. M.; Record, M. T. Partitioning of Atmospherically Relevant Ions between Bulk Water and the Water/Vapor Interface. *Proc. Natl. Acad. Sci. U. S. A.* **2006**, *103*, 14278−14281.
(92) Pegram, L. M.; Record, M. T. Quantifying Accumulation or Exclusion of H^+, HO^-, and Hofmeister Salt Ions near Interfaces. *Chem. Phys. Lett.* **2008**, *467*, 1−8.
(93) Callahan, K. M.; Casillas-Ituarte, N. N.; Xu, M.; Roeselova, M.; Allen, H. C.; Tobias, D. J. Effect of Magnesium Cation on the Interfacial Properties of Aqueous Salt Solutions. *J. Phys. Chem. A* **2010**, *114*, 8359−8368.
(94) Bian, H.-t.; Feng, R.-r.; Xu, Y.-y.; Guo, Y.; Wang, H.-f. Increased Interfacial Thickness of the NaF, NaCl and NaBr Salt Aqueous Solutions Probed with Non-Resonant Surface Second Harmonic Generation (SHG). *Phys. Chem. Chem. Phys.* **2008**, *10*, 4920−4931.
(95) Verreault, D.; Allen, H. C. Bridging the Gap between Microscopic and Macroscopic Views of Air/Aqueous Salt Interfaces. *Chem. Phys. Lett.* **2013**, *586*, 1−9.
(96) Ong, S. W.; Zhao, X. L.; Eisenthal, K. B. Polarization of Water Molecules at a Charged Interface - 2nd Harmonic Studies of the Silica Water Interface. *Chem. Phys. Lett.* **1992**, *191*, 327−335.
(97) Boxe, C. S.; Colussi, A. J.; Hoffmann, M. R.; Murphy, J. G.; Wooldridge, P. J.; Bertram, T. H.; Cohen, R. C. Photochemical Production and Release of Gaseous NO_2 from Nitrate-Doped Water Ice. *J. Phys. Chem. A* **2005**, *109*, 8520−8525.
(98) Gard, E. E.; Kleeman, M. J.; Gross, D. S.; Hughes, L. S.; Allen, J. O.; Morrical, B. D.; Fergenson, D. P.; Dienes, T.; Galli, M. E.; Johnson, R. J.; et al. Direct Observation of Heterogeneous Chemistry in the Atmosphere. *Science* **1998**, *279*, 1184−1187.
(99) Honrath, R. E.; Peterson, M. C.; Guo, S.; Dibb, J. E.; Shepson, P. B.; Campbell, B. Evidence of NO_x Production within or Upon Ice Particles in the Greenland Snowpack. *Geophys. Res. Lett.* **1999**, *26*, 695−698.
(100) Logan, J. A. Nitrogen Oxides in the Troposphere - Global and Regional Budgets. *J. Geophys. Res., C: Oceans Atmos.* **1983**, *88*, 785−807.
(101) Hunt, S. W.; Roeselova, M.; Wang, W.; Wingen, L. M.; Knipping, E. M.; Tobias, D. J.; Dabdub, D.; Finlayson-Pitts, B. J. Formation of Molecular Bromine from the Reaction of Ozone with Deliquesced NaBr Aerosol: Evidence for Interface Chemistry. *J. Phys. Chem. A* **2004**, *108*, 11559−11572.
(102) Hanson, D. R.; Ravishankara, A. R. Reactive Uptake of $ClONO_2$ onto Sulfuric Acid Due to Reaction with HCl and H_2O. *J. Phys. Chem.* **1994**, *98*, 5728−5735.
(103) Nissenson, P.; Knox, C. J. H.; Finlayson-Pitts, B. J.; Phillips, L. F.; Dabdub, D. Enhanced Photolysis in Aerosols: Evidence for Important Surface Effects. *Phys. Chem. Chem. Phys.* **2006**, *8*, 4700−4710.
(104) Textor, C.; Schulz, M.; Guibert, S.; Kinne, S.; Balkanski, Y.; Bauer, S.; Berntsen, T.; Berglen, T.; Boucher, O.; Chin, M.; et al. Analysis and Quantification of the Diversities of Aerosol Life Cycles within AeroCom. *Atmos. Chem. Phys.* **2006**, *6*, 1777−1813.
(105) Adams, E. M.; Allen, H. C. Palmitic Acid on Salt Subphases and in Mixed Monolayers of Cerebrosides: Application to Atmospheric Aerosol Chemistry. *Atmosphere (Basel)* **2013**, *4*, 315−336.